Journal of Sound and Vibration (2002) **253**(2), 347–358
doi:10.1006/jsvi.2001.4004, available online at http://www.idealibrary.com on IDEAL®

A VIBRO-IMPACTING MODEL FOR THE DETECTION OF DELAMINATION

P. VIELSACK

Institut für Mechanik, Universität Karlsruhe, Postfach 6980, 76131 *Karlsruhe, Germany.*
E-mail: peter.vielsack@bau-verm.uni-karlsruhe.de

(*Received* 21 *March* 2001, *and in final form* 13 *July* 2001)

Forced oscillations of delaminated sandwich structures are dominated by impacts. A rigid body-spring model allows a discussion of the influence of internal dissipation on the system's response and the evolution of the number of impacts.

1. INTRODUCTION

The dynamical identification of delamination in sandwich structures is one of the main objectives of non-destructive testing for composites. A recently published review [1] gives numerous mechanical models, which are based on linear assumptions. As a counter example, consider a sandwich beam of length 307 cm with rectangular cross-section 4·7/5·0 cm. It consists of five laminae (Raminwood), where the lowest lamina is delaminated symmetrically along a length of 144 cm (see Figure 1). The beam is suspended by soft springs at the nodes of the lowest natural mode. Vibrations are induced by an unbalanced rotating mass of 25 g at the left end. The exciting Ω frequency can be adjusted up to a certain limit. The total mass of the exciting device is 1900 g. At the right end of the beam, the same counter mass leads to a horizontal equilibrium position of the whole system. In this state, the aperture along the delaminated zone has a maximum of 1·5 mm in the middle of the beam. During motion this gap opens and closes periodically. Each contact gives rise to an impact of both parts of the beam, which can be heard as a rattling noise.

An opto-electronical measure gives the mid-displacement x depending on the exciting frequency Ω (see Figure 2(a)). A break is caused by the Sommerfeld effect (weakdrive). The result does not exhibit any extraordinary phenomenon compared to well-known steady state amplitudes of linear systems.

A piezo film sensing device enables identification of the number N of impacts during one period of excitation and to prove the periodicity of their occurrence (see Figure 2(b)). On increasing the exciting frequency up to resonance, the number of impacts during one exciting period changes step by step. Near resonance two impacts exist. After the break, the motion becomes irregular. The number of impacts during one exciting period is no longer fixed and the motion is quasi-periodic. This is indicated by a dashed line in Figure 2(b).

The influence of the impacts on the motion can be identified by an acceleration meter. Figure 3 enables a comparison of the experimentally obtained acceleration amplitude spectra in a semi-logarithmic scale at resonance for the undamaged beam (Figure 3(a) and the beam with delamination (Figure 3(b)). Obviously, the occurence of impacts leads to a significant change in the properties of the oscillations.

0022-460X/02/$35.00

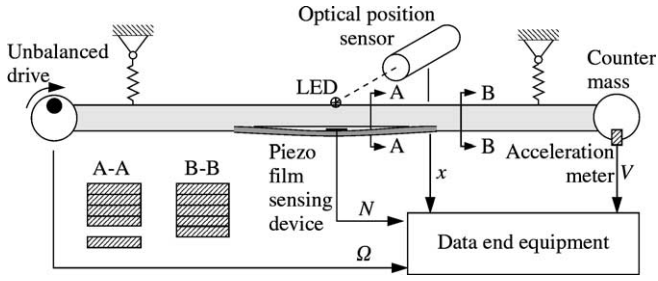

Figure 1. Scheme of the experimental set-up.

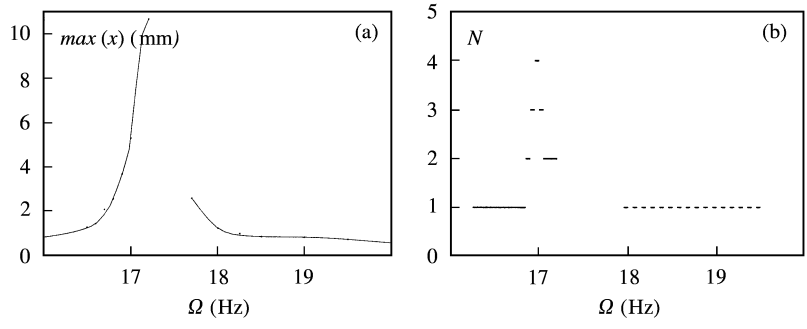

Figure 2. Response of the system: (a) steady state amplitudes, and (b) number of impacts.

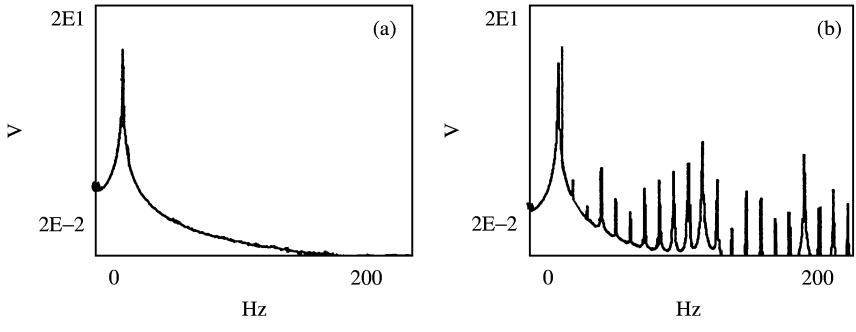

Figure 3. Amplitude-response spectra at resonance: (a) undamaged, and (b) delaminated.

The paradigm in the area of vibro-impacting is the motion of a rigid mass that collides with an oscillating stiff surface [2]. The existence and stability of subharmonic motions and non-linear phenomena, such as cascades of period doubling bifurcation and the existence of chaotic motion have been intensively investigated in many publications. The present major task, however, is to find the correlation between the exciting frequency and the corresponding evolution of the number of impacts, and the sensitivity of the non-linear system's responses on the coefficient of restitution and on the internal damping. For this purpose, a simple description of the mechanical behaviour of a delaminated beam is a major task. In the following, the concept of concentrated masses and stiffnesses gives a forced two-degree-of-freedom (d.o.f.) vibro-impacting system to capture the main phenomena.

2. MECHANICAL SYSTEM

Two neighbouring linear oscillators with stiffnesses k_1, k_2, masses m_1, m_2 and co-ordinates x_1, x_2 are considered. Internal energy dissipation is modelled by a coefficient of restitution e and viscous damping in both subsystems with constants d_1 and d_2. In a state of rest, both masses touch each other without prestressing. The springs are fixed at the two opposite sides of a box, which is harmonically driven with amplitude a and angular frequency Ω (see Figure 4).

On shaking the box, discontinuities of the motion occur due to impacts and sudden changes in the system's behaviour. A solution is put together by a sequence of different states

$$x_i = \begin{cases} x_i^{(1)} \;;\; t^{(1)} \leqslant t < t^{(2)}, & \\ x_i^{(2)} \;;\; t^{(2)} \leqslant t < t^{(3)}, & i = 1, 2, \\ \vdots \quad ; \; \vdots & k = 1, 2, 3, 4 \ldots . \\ x_i^{(k)} \;;\; t^{(k)} \leqslant t < t^{(k+1)}, & \end{cases} \tag{1}$$

The kth state is valid in the unknown interval $t^{(k)} \leqslant t < t^{(k+1)}$. The distinct time $t^{(k)}$ is named the kth separation time. To obtain a non-dimensional representation of all equations of motion the ratios

$$\omega^2 = k_1/m_1, \qquad \eta = \Omega/\omega, \qquad \mu = m_2/m_1, \qquad \kappa = k_2/k_1 \tag{2}$$

are introduced. For a systematic treatment of all possible states, the use of a third co-ordinate $x_3(t)$ for the state $x_1(t) \equiv x_2(t) = x_3(t)$ is recommended. This gives the non-dimensional displacements relative to the box

$$\xi_i^{(k)} = x_i^{(k)}/a\eta^2, \quad i = (1 \wedge 2) \vee 3. \tag{3}$$

A non-dimensional time

$$\tau = \omega t - \tau_s^{(k)} \tag{4}$$

starts in the kth state with $\tau = 0$. The end of this state is reached at $\tau = \tau_e^{(k)}$. In the subsequent $(k + 1)$th state, the new separation time must be updated by

$$\tau_s^{(k+1)} = \tau_s^{(k)} + \tau_e^{(k)}. \tag{5}$$

The distinct equations of motion valid for $0 \leqslant \tau < \tau_e^{(k)}$ must be selected from the set

$$\xi_i''^{(k)} + 2D_i\xi_i'^{(k)} + \omega_i^2\xi_i^{(k)} = \sin\eta(\tau + \tau_s^{(k)}), \quad i = (1 \wedge 2) \vee 3, \quad k = 1, 2, 3, 4 \ldots \tag{6}$$

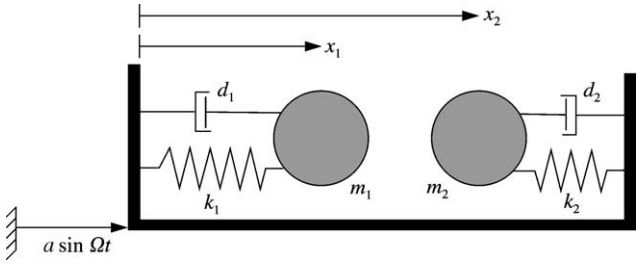

Figure 4. Scheme of the mechanical system.

with non-dimensional squares of the natural frequencies

$$\omega_1^2 = 1, \qquad \omega_2^2 = \kappa/\mu, \qquad \omega_1^2 = (1+\kappa)/(1+\mu) \tag{7}$$

and damping

$$D_1 = d_1/2\omega m_1, \qquad D_2 = d_2/2\omega m_2, \qquad D_3 = (d_1+d_2)/2\omega(m_1+m_2). \tag{8}$$

Each initial value problem starting at $\tau = 0$ needs the conditions

$$\left.\begin{aligned} \xi_i^{(k)}(0) &= c_i^{(k)} \\ \xi_i'^{(k)}(0) &= v_i^{(k)} \end{aligned}\right\} \quad i = (1 \wedge 2) \vee 3. \tag{9}$$

They are assumed to be known from the history of motion, which means from the end of the preceding state. Considering equation (9), the explicit solution of equation (6) is

$$\xi_i^{(k)} = a_i \cos\eta(\tau + \tau_s^{(k)}) + b_i \sin\eta(\tau + \tau_s^{(k)}) + \mathrm{e}^{-D\tau}(\alpha_i^{(k)} \cos\kappa_i\tau + \beta_i^{(k)} \sin\kappa_i\tau) \tag{10}$$

with the constants

$$\begin{aligned} a_i &= -\frac{2D_i\eta}{(\omega_i^2-\eta^2)^2 + (2D_i\eta)^2}, \qquad b_i = \frac{\omega_i^2-\eta^2}{(\omega_i^2-\eta^2)^2 + (2D_i\eta)^2}, \\ v_i &= \sqrt{\omega_i^2 - D_i^2}, \qquad \alpha_i^{(k)} = c_i^{(k)} - (a_i \cos\eta\tau_s^{(k)} + b_i \sin\eta\tau_s^{(k)}), \\ \beta_i^{(k)} &= \frac{1}{v_i}\,[v_i^{(k)} + D_i\alpha_i^{(k)} - \eta(b_i \cos\eta\tau_s^{(k)} - a_i \sin\eta\tau_s^{(k)})]. \end{aligned} \tag{11}$$

Now assume as the first possibility a motion where both masses are separated. Their relative displacement is

$$\xi_2^{(k)}(\tau) - \xi_1^{(k)}(\tau) \neq 0, \quad \tau > 0. \tag{12}$$

An impact occurs under the condition

$$\xi_2^{(k)}(\tau) - \xi_1^{(k)}(\tau) = 0. \tag{13}$$

The first root in the open interval $\tau > 0$ of the transcendental algebraic equation (13) gives the time $\tau_e^{(k)}$ and from equation (5), the new separation time in the subsequent $(k+1)$th state. Moreover, the initial conditions (9) for the displacements in the $(k+1)$th state can be calculated from

$$c_i^{(k+1)} = \xi_i^{(k)}(\tau_e^{(k)}), \quad i = (1 \wedge 2) \vee 3. \tag{14}$$

To obtain the initial conditions for the velocities, the impact must be considered. Following Newton's assumption of a sudden impact with a restitution coefficient e yields

$$\begin{aligned} v_1^{(k+1)} &= \xi_1'^{(k)}(\tau_e^{(k)}) - \frac{(1+e)\mu}{(1+\mu)}[\xi_1'^{(k)}(\tau^{(k)})_e - \xi_2'^{(k)}(\tau_e^{(k)})], \\ v_2^{(k+1)} &= \xi_2'^{(k)}(\tau_e^{(k)}) + \frac{(1+e)\mu}{(1+\mu)}[\xi_1'^{(k)}(\tau_e^{(k)}) - \xi_2'^{(k)}(\tau_e^{(k)})]. \end{aligned} \tag{15}$$

In the case of a zero relative velocity

$$v_2^{(k+1)} - v_1^{(k+1)} \equiv 0, \tag{16}$$

the $(k+1)$th state is a motion with both masses in permanent contact. For all non-vanishing restitution coefficients, equality (16) can lead to a sequence of infinite numbers of impacts with a corresponding sequence of time intervals tending to zero.

Therefore, the weaker unequality

$$v_2^{(k+1)} - v_1^{(k+1)} < \gamma, \quad \gamma \ll 1 \tag{17}$$

will allow a decision on whether a state with permanent contact follows on impact.

Next, assume a second possibility, namely the kth state is a motion of both masses in contact for $\tau > 0$, which implies a compressive force $F < 0$ between both masses. A free-body diagram yields the non-dimensional representation $f^{(k)} = (m_1 + m_2)F/a\Omega^2 m_1 m_2$ of the contact force

$$f^{(k)} = 2(D_1 - D_2)\xi_3' + (\omega_1^2 - \omega_2^2)\xi_3. \tag{18}$$

The first root of the transcendental algebraic equation

$$f^{(k)}(\tau) = 0 \tag{19}$$

in the open interval $\tau > 0$ gives the end $\tau_e^{(k)}$ of the kth state. Knowing $\tau_e^{(k)}$ all initial conditions for the subsequent $(k + t)$th state of a separated motion can be calculated from

$$\begin{aligned} c_1^{(k+1)} &= c_2^{(k+1)} = \xi_3^{(k)}(\tau_e^{(k)}), \\ v_1^{(k+1)} &= v_2^{(k+1)} = \xi_3'^{(k)}(\tau_e^{(k)}). \end{aligned} \tag{20}$$

On summarizing the above, it is clear that no numerical integration is needed. The actual problem is the numerical calculation of roots of algebraic equations with sufficient accuracy to avoid unstable results [3]. Despite the fact that each state $x_i^{(k)}$ is described explicitly by linear equations, the calculation of the sequence of separation times therefore turns the whole problem into a strongly non-linear one. Smooth mechanical systems with n d.o.f. need $2n$ initial conditions at the beginning of motion. The considered system additionally requires a starting value $\tau_s^{(1)}$ and a choice about the properties of the first state.

3. ELASTIC IMPACT AND SMALL INTERNAL DAMPING

Only in the exceptional case $m_1 = m_2$, $k_1 = k_2$ and $d_1 = d_2$ do both masses vibrate harmonically without influencing each other. In the following, a slightly distuned system with $m_1 = m_2$, $d_1 = d_2$ but $k_2 = k_1 = 1{\cdot}2$ will be considered. Then, the natural frequencies of both linear subsystems differ by about 10%. This assumption seems to capture the most unfavourable situation. It corresponds to a beam with a rectangular cross-section which is delaminated along its mid-plane without any aperture along the border in the state of static equilibrium.

The oscillation of the masses m_1 and m_2 are described by co-ordinates ξ_1, ξ_1' and ξ_2, ξ_2' respectively. The number of four variables can be reduced to two by introducing relative co-ordinates

$$\xi_{Rel} = \xi_2 - \xi_1, \qquad \xi_{Rel}' = \xi_2' - \xi_1'. \tag{21}$$

The consequences with respect to the graphical illustration of the results will be discussed exemplarily for a stationary oscillation with frequency ratio $\eta = 0{\cdot}4$, $D = 0{\cdot}005$ and a restitution coefficient $e = 0{\cdot}7$.

The phase plot for each mass gives two closed loops in Figure 5(a). Three states can be clearly seen: both masses move separately from each other, a sequence of impacts occurs and both masses move in permanent contact. To identify the transition to permanent contact by equation (17), $\gamma = 10^{-4} \max\xi_{Rel}'$ is used. Figure 5(b) exhibits the same situation in relative co-ordinates. The phase plot for one response period consists of many loops.

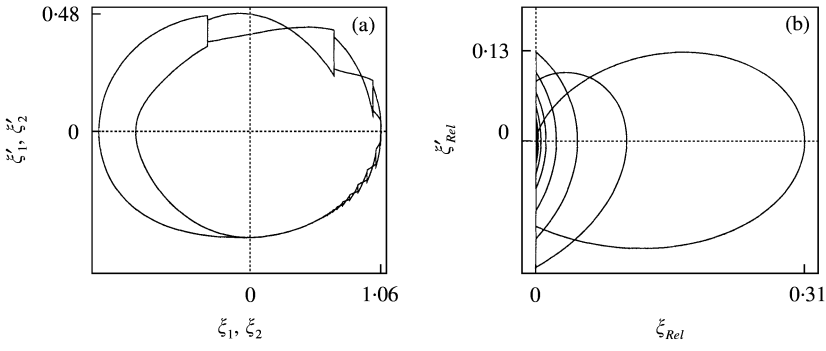

Figure 5. Phase curves for $\eta = 0{\cdot}4$; $e = 0{\cdot}7$; $D = 0{\cdot}005$. (a) Motion of both masses and (b) relative motion.

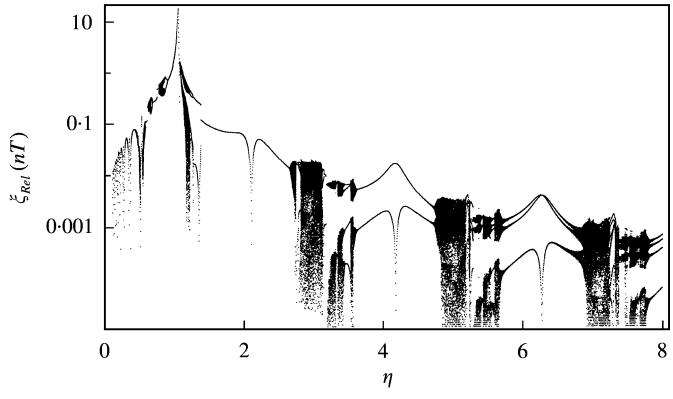

Figure 6. Bifurcation diagram for $e = 0{\cdot}7$; $D = 0{\cdot}005$.

Each loop begins and ends at an impact, which corresponds to a jump of the phase curve along the axis of velocity. The state with permanent contact is contracted to a point at the origin. In the following only relative co-ordinates will be used. For further discussions, the non-dimensional periodical time of the excitation

$$T = \eta/2\pi \tag{22}$$

is also introduced.

3.1. BIFURCATION

A restitution coefficient $e = 0{\cdot}7$ describes an impact close to an ideal elastic one. In addition, with $D = 0{\cdot}005$ the system has a low dissipation.

The frequency ratio η is chosen as the sole varied parameter with increments $\Delta\eta = 0{\cdot}001$ for constructing a bifurcation diagram in the range $0{\cdot}1 \leqslant \eta \leqslant 8{\cdot}0$ in a semi-logarithmic scale Figure 6. The Poincaré-sections method is used to collect samples of responses of the relative displacement, denoted $\xi_{Rel}(nT)$, in a number of $n = 500(1)700$ excitation periods. After finishing a distinct calculation for a certain value η, all results at the end are taken as initial conditions for the next calculation with $\eta + \Delta\eta$. In this way, the necessary number $n = 500$ for the elimination of transient effects can be kept relatively small.

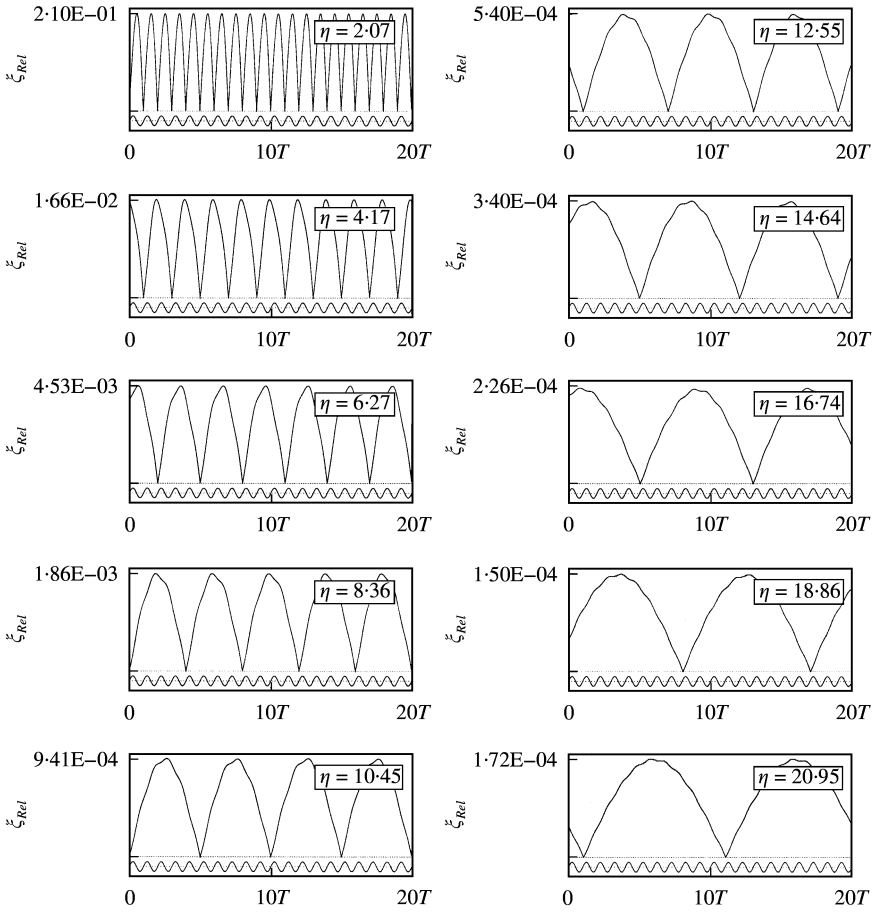

Figure 7. Multiplicity of periodic responses at relative resonance peaks.

In the range $\eta < 0{\cdot}43$, the oscillations are T-periodic with states of permanent contact, equivalent to the example given in Figure 5. These states of permanent contact vanish for all larger values of η. Then, the typical feature of the bifurcation diagram is an alternation of regions of irregularity and windows of periodic responses. Their multiplicity with respect to the excitation period T increases by steps of one T.

The corresponding time-displacement diagrams for the relative resonance peaks within the windows are plotted in Figure 7 in a time range of $20T$, using different scales on the ordinates. To allow a comparison between input and output, the harmonic excitation is additionally given in the lower curve. All periodic responses show one impact during one response period. It is worth noting that a shift from one window to the next increases not only the number of periods by steps of one T, but also the corresponding time distance between two successive impacts is enlarged by one T. This fact is the key for a discussion about the nature of regions of irregularity.

3.2. INFLUENCE OF IMPACTS

The typical features of a motion are strongly affected by the sequence of the corresponding impacts. The latter are not visible in a bifurcation diagram. Therefore, phase

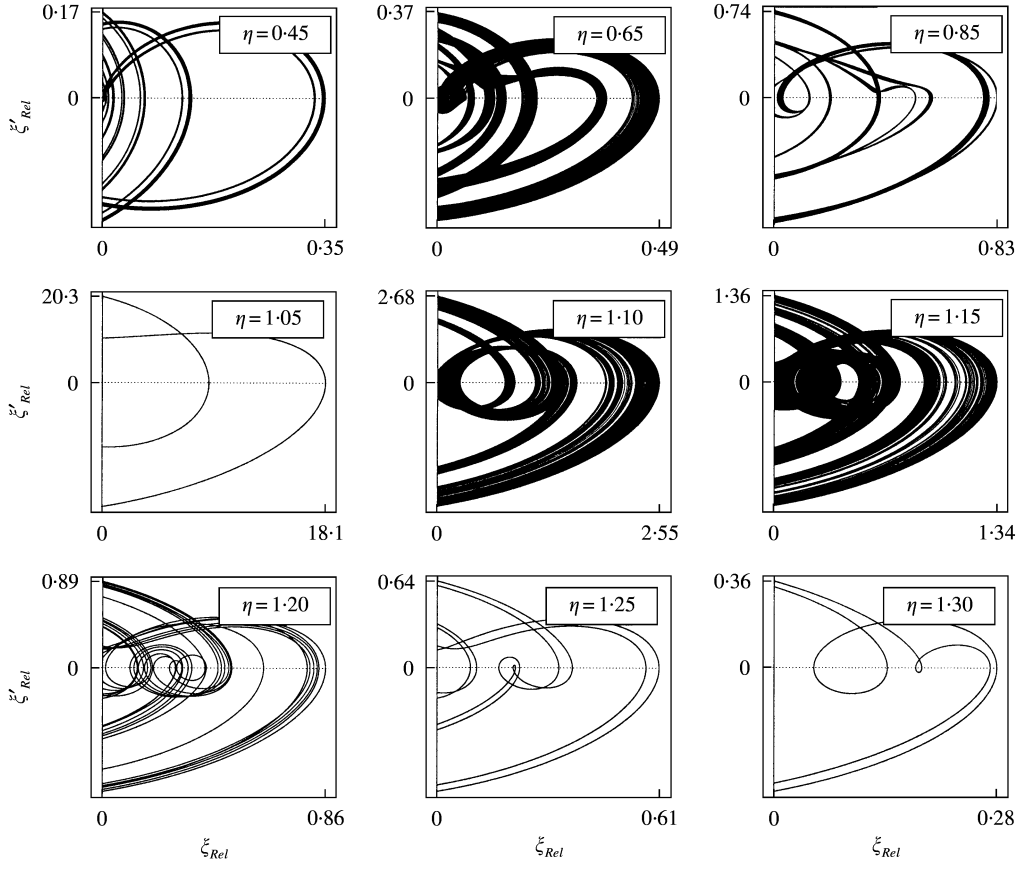

Figure 8. Typical phase curves in the first irregular region $0{\cdot}43 < \eta < 1{\cdot}37$.

curves are needed. To get a curve for a given η, a time range of $2500T$ is calculated, $2000T$ are omitted to eliminate the influence of the initial conditions and only the result of the last $500T$ is plotted. Periodic responses show a distinct quantity of lines. In the case of quasi-periodic oscillations, the lines are widened up to stripes of different widths.

Firstly, the properties of the oscillations in the first region of irregularity $0{\cdot}43 < \eta < 1{\cdot}37$ will be considered in detail. In Figure 8 some typical results are given, using different scales on both axes for different values of η.

On increasing η, ranges with bifurcated and quasi-periodic oscillations interchange with the dominant feature, so that the number of impacts during one T decreases. Then, the diminishing of the number of impacts leads for $n \geqslant 0{\cdot}89$ to a T-periodic response with two impacts during one T. The absolute resonance peak $\max \xi_{Rel} = 21{\cdot}56$ is found at $\eta = 1{\cdot}045$. Contrary to expectations, the resonance points $\eta = 1{\cdot}0$ and $1{\cdot}095$ of both linear subsystems have no influence at all. Starting with $\eta \geqslant 1{\cdot}07$, again bifurcated and quasi-periodic oscillations interchange. Coarse analysis enables them all to be identified as approximately $2T$-periodic. The impacts are distributed irregularly. In addition, non-unique solutions are found.

The second region of irregularity occurs for values $2{\cdot}61 < \eta < 3{\cdot}77$. Both neighbouring windows of periodical solutions with periods T and $2T$, respectively, exhibit only one impact in a response period. This time shifting of the impact causes a region of quasi periodical oscillations with an irregular distribution of the impacts. Some typical phase curves illustrate this transition in Figure 9.

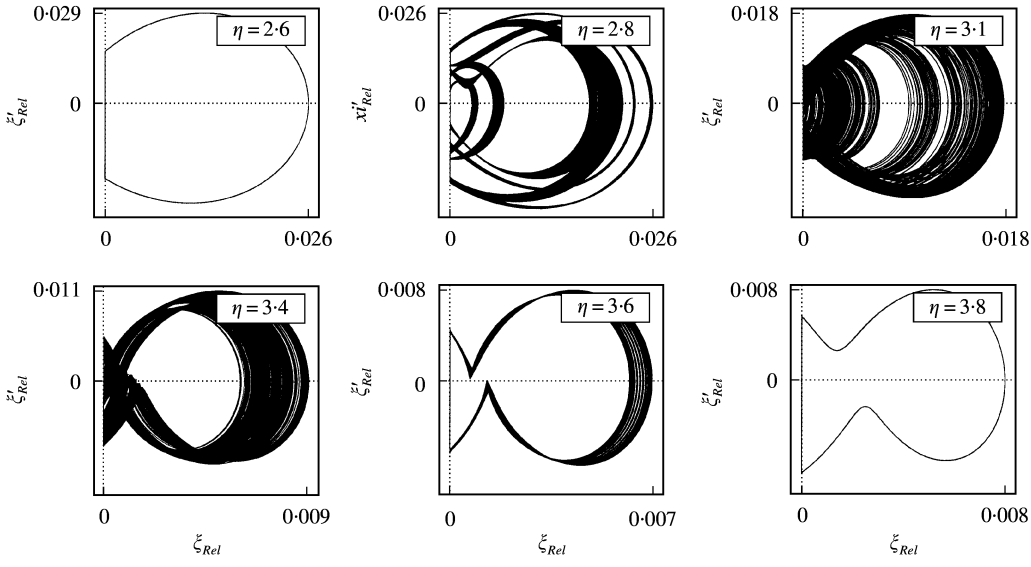

Figure 9. Typical phase curves in the second irregular region $2{\cdot}61 < \eta < 3{\cdot}77$.

As expected, all other irregular regions in Figure 6 show a similar evolution when shifting from one window to the next. All irregularities occur when increasing the response period by one T and keeping the number of impacts fixed to one in a response period. As a result, bifurcation diagrams cannot provide full information about motions with impacts. Even the common assertion that the onset of chaos starts at "dark" regions is disproved.

On summarizing all the results with respect to the detection of delamination in sandwich structures, significant signals caused by intensive impacts can be expected in the vicinity of the absolute resonance peak at $\eta = 1{\cdot}045$. The corresponding impulses, which are proportional to the jump of the relative velocity ξ'_{Rel}, are extremal, as can be seen in Figures 8 and 9. On increasing η, both relative displacement and velocity diminish by powers of 18. In a first approximation, these oscillations resemble those of a single-d.o.f. system without any separation of both masses.

4. HIGH DISSIPATION

In contrast to the preceding assumption of a low dissipation, the influence of a high dissipation on the system's behaviour will be considered now. This can be achieved either with a significant internal damping and a large restitution coeffcient close to an elastic impact or a low restitution coefficient close to a plastic impact combined with low internal damping.

4.1. ELASTIC IMPACT AND LARGE DAMPING

The calculations are performed with $e = 0{\cdot}7$ and a damping parameter $D = 0{\cdot}05$ which is 10 times larger than before. The corresponding bifurcation diagram is plotted in Figure 10.

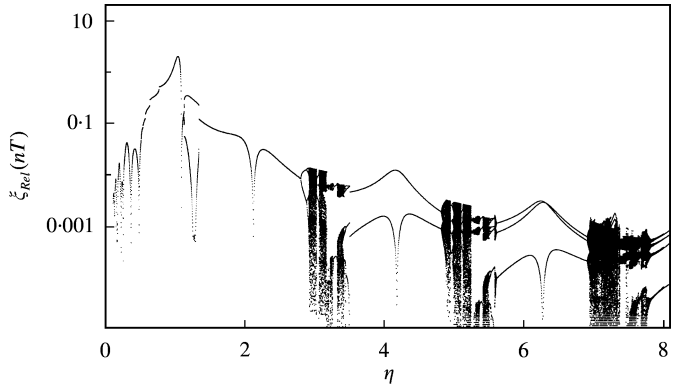

Figure 10. Bifurcation diagram for $e = 0{\cdot}7$ and $D = 0{\cdot}05$.

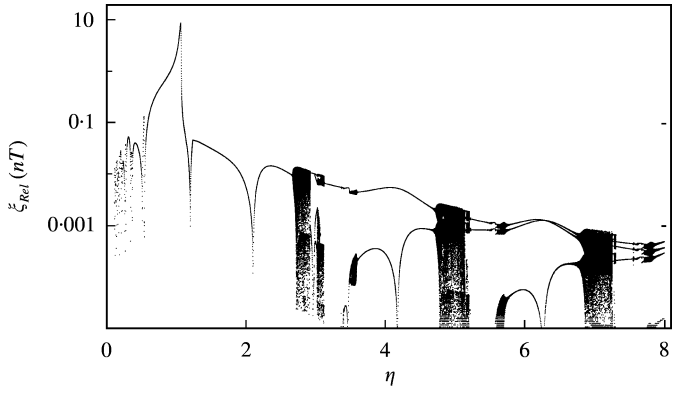

Figure 11. Bifurcation diagram for $e = 0{\cdot}3$ and $D = 0{\cdot}005$.

The evolution of the multiplicity of the response periods and the corresponding number of impacts is as follows:

$\eta < 0{\cdot}48$: T-periodic, states of permanent contact, sequence of impacts.
$0{\cdot}48 < \eta < 0{\cdot}85$: T-periodic, diminution of impacts from seven to two.
$0{\cdot}85 < \eta < 1{\cdot}08$: T-periodic, two impacts, $\max \xi_{Rel} = 2{\cdot}63$ at $\eta = 1{\cdot}056$.
$1{\cdot}08 < \eta < 1{\cdot}1$: T-periodic, one impact.
$1{\cdot}11 < \eta < 1{\cdot}33$: $2T$-perodic, three impacts, non-unique solutions are found.
$\eta > 1{\cdot}33$: in principle the same properties as discussed for $e = 0{\cdot}7$ and $D = 0{\cdot}005$.

It must be mentioned, that increasing the value D further eliminates the bifurcation within the range $1{\cdot}11 < \eta < 1{\cdot}33$ in such a way that the responses become T-periodic with one impact. On summarizing, high dissipation caused by large internal damping does not change the dominant features of the evolution of bifurcation. Only the first irregular region is eliminated and turned over to periodic responses.

4.2. PLASTIC IMPACT AND LOW DAMPING

The calculations are performed with $e = 0{\cdot}3$ close to the exceptional case of a plastic impact. The damping parameter $D = 0{\cdot}005$ is small. The corresponding bifurcation diagram can be seen in Figure 11.

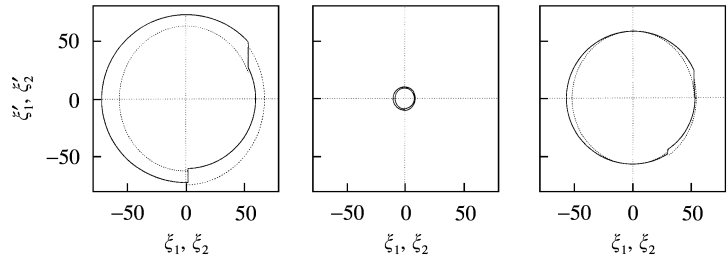

Figure 12. Phase curves of both masses at the main resonance peak: (a) close to elastic impact, low internal damping $D = 0{\cdot}005$; (b) close to elastic impact, significant internal damping $D = 0{\cdot}05$; and (c) close to plastic impact, low internal damping $D = 0{\cdot}005$.

The evolution of the different responses on increasing η is as follows:

$\eta < 0{\cdot}97$: T-periodic, states of permanent contact, sequence of impacts.
$0{\cdot}97 < 1{\cdot}02$: T-periodic, three impacts.
$1{\cdot}02 < \eta < 1{\cdot}23$: T-periodic, two impacts, $\max \xi_{Rel} = 16{\cdot}41$ at $\eta = 1{\cdot}048$.
$1{\cdot}23 < \eta < 1{\cdot}37$: T-periodic, one impact.
$\eta > 1{\cdot}37$: in principle the same properties as discussed for $e = 0{\cdot}7$ and $D = 0{\cdot}005$.

As before, only the range of lower values of η is significantly affected by a small restitution coefficient. Mainly, the range of motions with states of permanent contact is enlarged. The global evolution of bifurcation still exists.

5. CONCLUSION

Vibrotesting of delaminated sandwich structures is based on a comparison of typical responses of the non-damaged and the delaminated system respectively. The considered two degree of freedom model allows a general discussion of the evolution of different types of oscillations and the corresponding number of impacts, depending on the exciting frequency. Experimental investigations need significant signals, which means that the amplitudes of both vibrating masses and the impulses of the corresponding impacts must be as large as possible. As has been shown, both conditions are fulfilled at the main resonance peak. On recapitulating the results, Figure 12 depicts the phase curves corresponding to the three considered cases with different dissipations. A continous line describes the T-periodic motion of the mass m_1 with generalized co-ordinates ξ_1 and ξ'_1, and a dotted line shows the motion of m_2 with ξ_2 and ξ'_2. A jump indicates an impact. Its magnitude is proportional to the impulse, which can be detected easily by experimental means. All pictures have the same scale.

On comparing Figures 12(a) and 12(b), significant internal damping in a delaminated structure is disadvantageous with respect to the detection of delamination by way of investigating the impacts. The vibrational amplitudes and the intensity of the impulses are low in Figure 12(b). In contrast, the dissipation caused by impacts with different restitution coefficients has a minor influence. A change from an impact with low dissipation (Figure 12(a)) to a high one (Figure 12(c)) gives results of the same order with regard to the impulses.

REFERENCES

1. Y. ZOU, L. TONG and G. P. STEVEN 2000 *Journal of Sound and Vibration* **230**, 357–378. Vibration based model-dependent damage (delamination) indentification and health monitoring for composite structures—a review.
2. P. J. HOLMES 1982 *Journal of Sound and Vibration* **84**, 173–189. The dynamics of repeated impacts with a sinussoidally vibrating table.
3. P. VIELSACK and A. HARTUNG 1999 *Zeitschrift für Angewandte Mathematik und Mechanik* **79**, 389–397. An example for the orbital stability of permanently disturbed non-smooth motions.